Neutron diffraction measurements of residual stresses around a crack tip developed under variable-amplitude fatigue loadings

Lee, S. Y.; Rogge, R. B.; Choo, H.; Liaw, P. K.

Publisher's version / Version de l'éditeur:
https://doi.org/10.1111/j.1460-2695.2010.01490.x
Fatigue & Fracture Of Engineering Materials & Structures, 33, 12, pp. 822-831, 2010-12-01

Fatigue & Fracture of
Engineering Materials & Structures

doi: 10.1111/j.1460-2695.2010.01490.x

Neutron diffraction measurements of residual stresses around a crack tip developed under variable-amplitude fatigue loadings

S. Y. LEE[1], R. B. ROGGE[2], H. CHOO[1] and P. K. LIAW[1]

[1]*Department of Materials Science and Engineering, The University of Tennessee, Knoxville, TN 37996, USA,* [2]*Canadian Neutron Beam Centre, National Research Council Canada, Chalk River, Ontario, Canada K0J 1J0*

Received in final form 19 April 2010

ABSTRACT The spatially resolved neutron-diffraction residual stress mappings were performed on five compact-tension (CT) specimens subjected to various variable-amplitude fatigue loadings (e.g. overload, underload and their mixed loads) during fatigue crack propagation. Three principal residual-stress components (i.e. longitudinal, transverse and normal stresses) were measured as a function of the distance from the crack tip along the crack-propagation direction. The shape of respective crack tips on the five CT specimens was examined using scanning electron microscope. The results show the distinct residual-stress fields near the crack tip and significant changes in the crack-tip geometry for five different loading cases. It is thought that the combined effects of the changes in the residual-stress state and crack-tip geometry seem to be a key factor to account for the observed transient crack-growth phenomena.

Keywords crack tip; fatigue crack propagation; neutron diffraction; residual stress; variable-amplitude fatigue.

INTRODUCTION

In the case of numerous fatigue-critical structure components, fatigue crack propagation under service conditions generally involves random or variable-amplitude loadings rather than constant-amplitude loading.[1] The accurate understanding and control for the crack resistance of materials subjected to variable-amplitude loadings, for example, overload and/or underload, are therefore crucial to develop the damage tolerance design and lifetime prediction methodology.

Residual stresses are one of the contributory factors to failure in structural components. Withers[2] demonstrated that when unexpected failure occurs it is often because residual stresses have combined critically with the applied stresses, or because they, together with the presence of unknown defects or poor microstructures, have dangerously lowered the applied stresses at which failure will occur. Residual stresses also play a significant role in the fatigue crack growth behaviour. It is generally known that compressive residual stresses are found to decrease the crack propagation rates, whereas tensile residual stresses yield the opposite effect.[3] More specifically, in terms of the crack-growth retardation phenomena following a single tensile overload, many researchers reported that the enlarged compressive residual stresses after a tensile overload are one of the possible retardation mechanisms, slowing down the crack-growth rates in the retardation period.[4–7] Makabe *et al*.[8] demonstrated that the tensile residual stresses developed by a compressive underload are an important consequence of the reversed plastic flow, leading to the reduction of crack-opening level and acceleration of crack-growth rate.

Various models depending on the residual stresses have also been developed to predict the fatigue crack growth behaviour under constant-amplitude or variable-amplitude loadings.[9,10] However, Lam *et al*.[11] pointed out that the models predicting the residual-stress effect on fatigue crack growth have not been completely quantified, due to a task of difficulty to accurately measure the residual-stress distribution. Thus, the direct residual-stress measurements near the crack tip influenced by prior plastic deformation will be of importance to the improvement of a fatigue lifetime prediction model, as well as a better understanding of the crack propagation behaviour.

Correspondence: P. K. Liaw. E-mail: pliaw@utk.edu

Nondestructive diffraction methods (e.g. high-energy synchrotron X-ray diffraction or neutron diffraction) are a powerful technique in the direct measurement of internal strains/stresses in the bulk sample.[12–20] Steuwer *et al*.[15] investigated the imaging of fatigue cracks and associated crack-tip strain field using synchrotron X-ray diffraction and tomography. They observed a significant compressive zone at and behind the crack tip following a 100% overload. Croft *et al*.[16] examined the local strain fields in the vicinity of fatigue-crack tips during *in situ* loading using synchrotron X-ray diffraction. They found a large compressive residual strain near the crack tip immediately after the overload, but there was no difference between the strain change ($\Delta\varepsilon_{yy}$) curves before and immediately after the overload. They also reported the transfer of load response between the overload position and the propagated crack tip following the overload. More recently, Lee *et al*.[20] showed the development of internal strains around a crack tip during tensile overloading, compressive underloading, and their combinations using neutron diffraction.

In this investigation, the direct measurements of residual-stress distribution are carried out as a function of the distance from the crack tip using neutron diffraction, immediately after applying the same loading conditions as our previous study[20] (i.e. a tensile overload, a compressive underload and their mixed loads during fatigue crack growth). The shape of respective crack tips for the different loading cases was examined using scanning electron microscope. The results will be useful for the development of more accurate residual-stress-based prediction models, as well as the computational simulations.

EXPERIMENTAL DETAILS

The fatigue crack growth experiments were conducted on a nickel-based HASTELLOY C-2000 (56%Ni–23%Cr–16%Mo, in weight percent)[21] compact-tension specimen (Fig. 1a) prepared according to the American Society for Testing and Materials (ASTM) Standards E647-99.[22] This material has a single-phase face-centered cubic (FCC) structure, yield strength of 393 MPa, Young's modulus of 207 GPa, ultimate tensile strength of 731 MPa and the average grain size of about 90 μm. The crack length was measured by crack-opening-displacement gauge using the compliance method. During the constant-amplitude fatigue crack growth [i.e. P_{max} = 8880 N, P_{min} = 89 N, a load ratio, R (P_{min}/P_{max}) = 0.01, and frequency = 10 Hz], one of the following loading conditions was applied at ΔK = 35.90 MPa·m$^{1/2}$. *Case 1*: continuously fatigue under the same baseline condition; *Case 2*: a single tensile overload (13 320 N, 150% of P_{max}); *Case 3*: a single compressive underload (−13 320 N); *Case 4*: overload–underload; and *Case 5*: underload–overload. After various loading conditions were applied, the constant-amplitude fatigue crack growth tests were resumed for all cases.

A neutron-diffraction residual stress mapping was performed on L3 spectrometer at Canadian Neutron Beam Centre, National Research Council Canada, Chalk River Laboratories, Canada. The five compact–tension (CT) specimens processed by the different loading conditions [i.e. constant-amplitude fatigued (*Case 1*), tensile overloaded (*Case 2*), compressive underloaded (*Case 3*), tensile overloaded–compressive underloaded (*Case 4*) and compressive underloaded–tensile overloaded (*Case 5*)] were prepared to study the influence of residual stresses on the crack growth rate, as shown in Fig. 2. Three principal residual-strain components [i.e. longitudinal (ε_x), transverse (ε_y) and normal (ε_z) strains, Fig. 1a] were measured as a function of the distance from the crack tip along the crack-growth direction (x-direction, Fig. 1b). A total of 26 points were measured as a function of the distance from the crack tip. To provide the required spatial resolution, the scanning intervals of 1 mm from −4 to 0 mm (crack tip), 0.5 mm from 0 to 8 mm where sharp strain gradients are expected, 2 mm from 8 to 16 mm, and 3 mm from 16 to 22 mm were employed.

A schematic view of the diffraction geometry is shown in Fig. 1c–e. For the longitudinal (ε_x) and transverse (ε_y) strain components (Fig. 1c and d, respectively), the wavelength of 1.31 Å was selected from the Ge115 monochromator. The specimen was aligned 53° (clockwise) from the incident neutron beam and the (311) diffraction pattern was measured in a stationary detector centred on a diffraction angle of $2\theta = 74°$. The longitudinal (ε_x) strain component was measured using 1-mm-wide and 2-mm-tall (parallel to y) incident beam slits, and 1-mm-wide diffracted beam slit. The transverse (ε_y) strain component was measured using 2-mm-wide and 1-mm-tall (parallel to x) incident beam slits, and 2-mm-wide diffracted beam slit.

For the normal (ε_z) strain component (Fig. 1e), the wavelength of 1.74 Å was chosen from the Ge115 monochromator. The specimen was aligned 127° (clockwise) from the incident neutron beam and the (311) diffraction pattern was recorded in a stationary detector centred on a diffraction angle of $2\theta = 106°$. Thus, the diffraction vectors were parallel to normal direction (parallel to z) of the specimen. The incident beam was defined by 2-mm-wide and 1-mm-tall (parallel to x) slits, and the diffracted beams were collimated by 2-mm-wide slit.

The interplanar spacings (d-spacings) along the longitudinal, transverse and normal directions were determined from the Gaussian fitting of the (311) diffraction peak and the lattice strains were obtained from

$$\varepsilon = (d - d_0)/d_0, \quad (1)$$

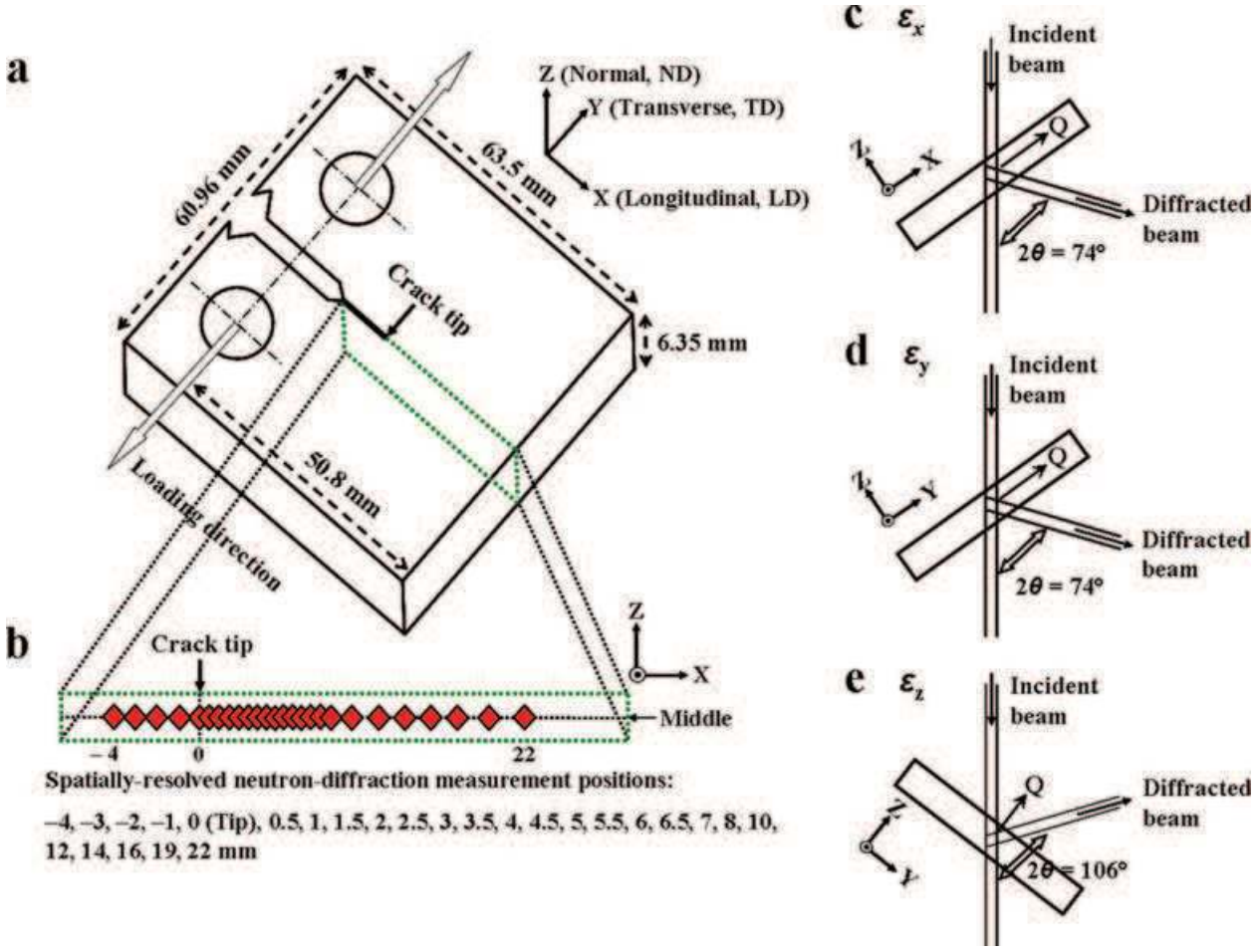

Fig. 1 (a) The geometry of a Hastelloy C-2000 compact–tension specimen; (b) spatially resolved neutron-diffraction measurement positions along the direction of crack propagation (x); schematic of diffraction geometry for the residual-stress mapping showing the scattering vector (Q) parallel to the coordinate (c) x: longitudinal strain (ε_x) component; (d) y: transverse strain (ε_y) component; (e) z: normal strain (ε_z) component.

where d_0 is the stress-free reference d-spacing, which was measured away from the crack tip. Three residual stress components, σ_i ($i = x$, y and z, corresponding to longitudinal, transverse and normal directions, respectively), are calculated from the three strain components using the following equation:

$$\sigma_i = \frac{E}{1+\nu}\left[\varepsilon_i + \frac{\nu}{1-2\nu}\left(\varepsilon_x + \varepsilon_y + \varepsilon_z\right)\right], \qquad (2)$$

where E (= 207 GPa) is the Young's modulus and ν (= 0.3) is the Poisson's ratio.

RESULTS AND DISCUSSION

Figure 3 shows the experimentally measured crack-propagation rate (da/dN) versus stress-intensity-factor range (ΔK) for five different loading cases. These results were previously reported, [20] and they were used to help understand the relationship between residual-stress distribution and crack-growth behaviour. The previous observations are summarized as follows: *Case 1* showed a linear increase of the crack-growth rate with increasing ΔK. After *Case 2* (a single tensile overload) was introduced, the crack-growth rate was instantaneously accelerated, and then a large crack-growth retardation period was observed. *Case 4* (overload–underload sequence) showed the significantly reduced crack-growth retardation, as compared to that of *Case 2*. On the other hand, after *Case 3* (a single compressive underload) was introduced, the crack-growth rate was initially accelerated, but the subsequent crack-growth rate was similar to that of *Case 1*. When *Case 5* (underload–overload sequence) was imposed, the crack-growth rates were similar to those of *Case 2*, indicating a large retardation period.

To obtain a better understanding of the transient crack-growth behaviour following the overload and/or underload, the residual stress fields near a fatigue-crack tip were

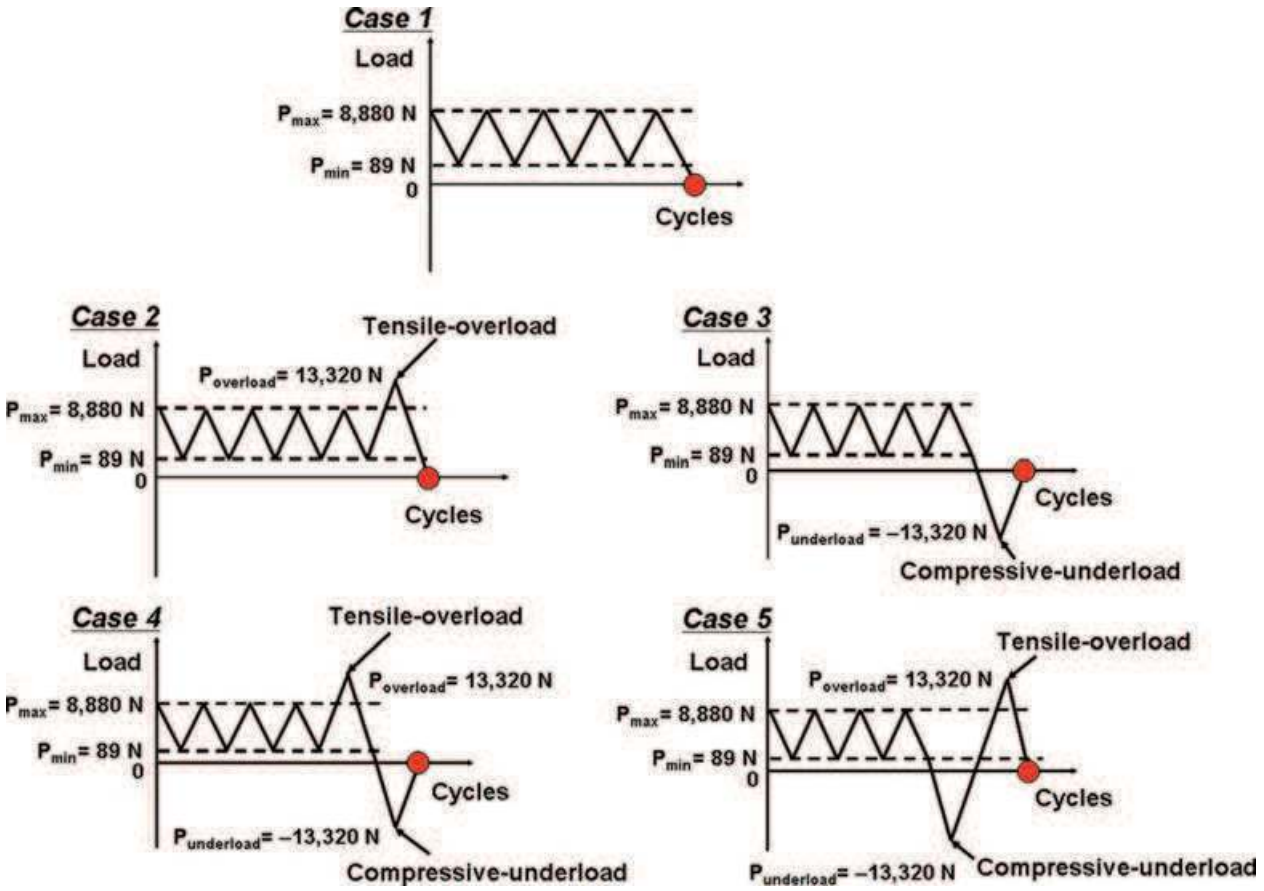

Fig. 2 Neutron residual-stress mappings shown in Fig. 1 were performed on the five compact–tension specimens subjected to various variable-amplitude fatigue-loading conditions (i.e. *Case 1*: constant–amplitude fatigued, *Case 2*: tensile overloaded, *Case 3*: compressive underloaded, *Case 4*: tensile overloaded–compressive underloaded and *Case 5*: compressive underloaded–tensile overloaded). Note that red-marked circles indicate the neutron measurement points.

measured using neutron diffraction, immediately after applying five different loading conditions, as shown in the marked points (Fig. 2). Figure 4 shows the longitudinal (σ_x), transverse (σ_y) and normal (σ_z) residual-stress profiles in the vicinity of the crack tip. In the case of *Case 1* (constant-amplitude fatigued), the tensile longitudinal residual stresses were examined behind the crack tip and the stresses were varied from tensile to compressive at about 0.5 mm ahead of the crack tip (Fig. 4a). The normal residual stress fields also showed similar stress distributions around the crack tip, as exhibited in Fig. 4e. The relatively large tensile residual stresses with a maximum of about 125 MPa were observed in a fatigue-wake region, and the sharp transition from tensile to compressive residual stresses was examined about 1 mm ahead of the crack tip. On the other hand, the transverse residual stresses showed the opposite trend. The compressive residual-stress fields with the maximum of about −70 MPa were observed behind of the crack tip and the tensile residual stresses were examined from about 1 to 8 mm in front of the crack tip. The monotonic plastic zone size of about 2.5 mm was estimated from the transverse residual-stress distribution ahead of the crack tip, as previously studied by Rice.[23] Compared to the thickness (6.35 mm) of the specimen, the cracks are in the predominant plane strain condition.

After *Case 2* (a single tensile overload) was applied, the residual stress fields near the crack tip were shown in Fig. 4a, c and e. It is noted that the application of tensile overload yielded large compressive residual stresses near the crack tip for the longitudinal component (Fig. 4a). For example, the tensile longitudinal residual stresses behind the crack tip observed in *Case 1* changed into the compressive residual stresses at −2.5 to 0 mm, and the larger compressive residual stresses were developed at 0 (crack tip, −123 MPa) to 3 mm. The effect of tensile overload on the transverse residual stresses was more significant. The large compressive residual stresses with a maximum of −225 MPa (at 0.5 mm) were observed within ±4 mm from the crack tip. The plastic zone size of about 5 mm at the overload was estimated from the residual stress profile in front of the crack tip (Fig. 4c). A tensile overload

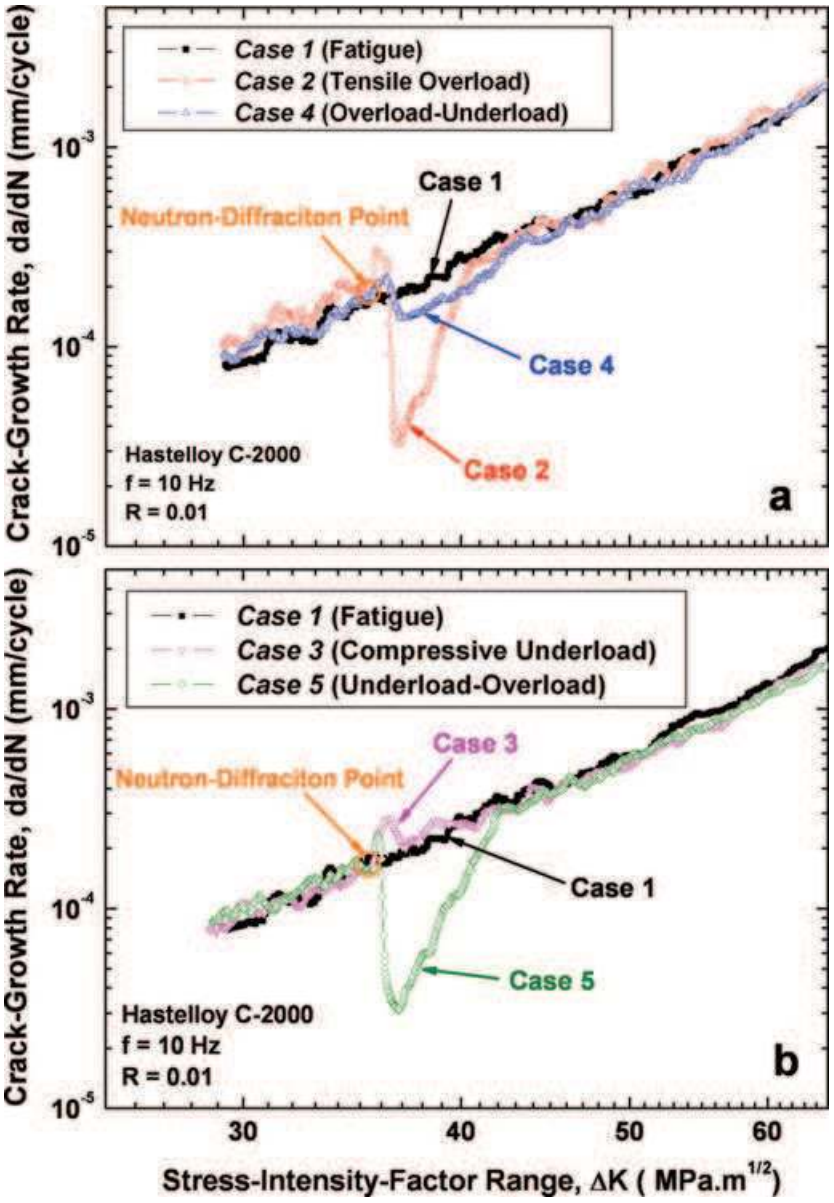

Fig. 3 The crack-growth rate (d*a*/d*N*) vs. stress-intensity-factor range (ΔK) for the tests with different loading cases. (a) *Case 1*, *Case 2* and *Case 4* and (b) *Case 1*, *Case 3* and *Case 5*. Note that the neutron residual-stress measurements were carried out at the marked circle points, which corresponds to those indicated in Fig. 2.

also influenced the normal residual-stress distributions, as shown in Fig. 4e. It was found that the tensile residual stresses examined in a fatigue-wake region of *Case 1* were significantly reduced. Especially, the tensile residual stresses of 105 MPa (*Case 1*) measured at the crack tip completely disappeared and became zero residual stress (*Case 2*), leading to a double-peak shape near the crack tip.

A compressive underload was imposed right after the tensile overload (*Case 4*) and the corresponding residual-stress profiles were shown in Fig. 4a, c and e. In Fig. 4a, the longitudinal residual-stress distributions showed a similar profile with those of *Case 1*. The large compressive residual stresses near the crack tip generated by the tensile overload changed into the tensile residual-stress fields by the compressive underload. A compressive underload also led to the relatively small compressive residual stresses within 4.5 mm in front of the crack tip for the transverse direction. The maximum compressive transverse residual stress of about −80 MPa was measured at 0.5 mm from the crack tip. Interestingly, the normal residual stress exhibited the distinct distributions with a wider double-peak shape. It was found that the first tensile maximum was at about 2 mm behind the crack tip, and the second one was at approximately 2.5 mm ahead of the crack tip. It might be due to the results of interaction between newly developed residual stress fields by non-uniform reverse plastic deformation and existing residual-stress fields. Based on the changes of residual-stress distribution, it can be thought that the zone of reverse plastic deformation by the

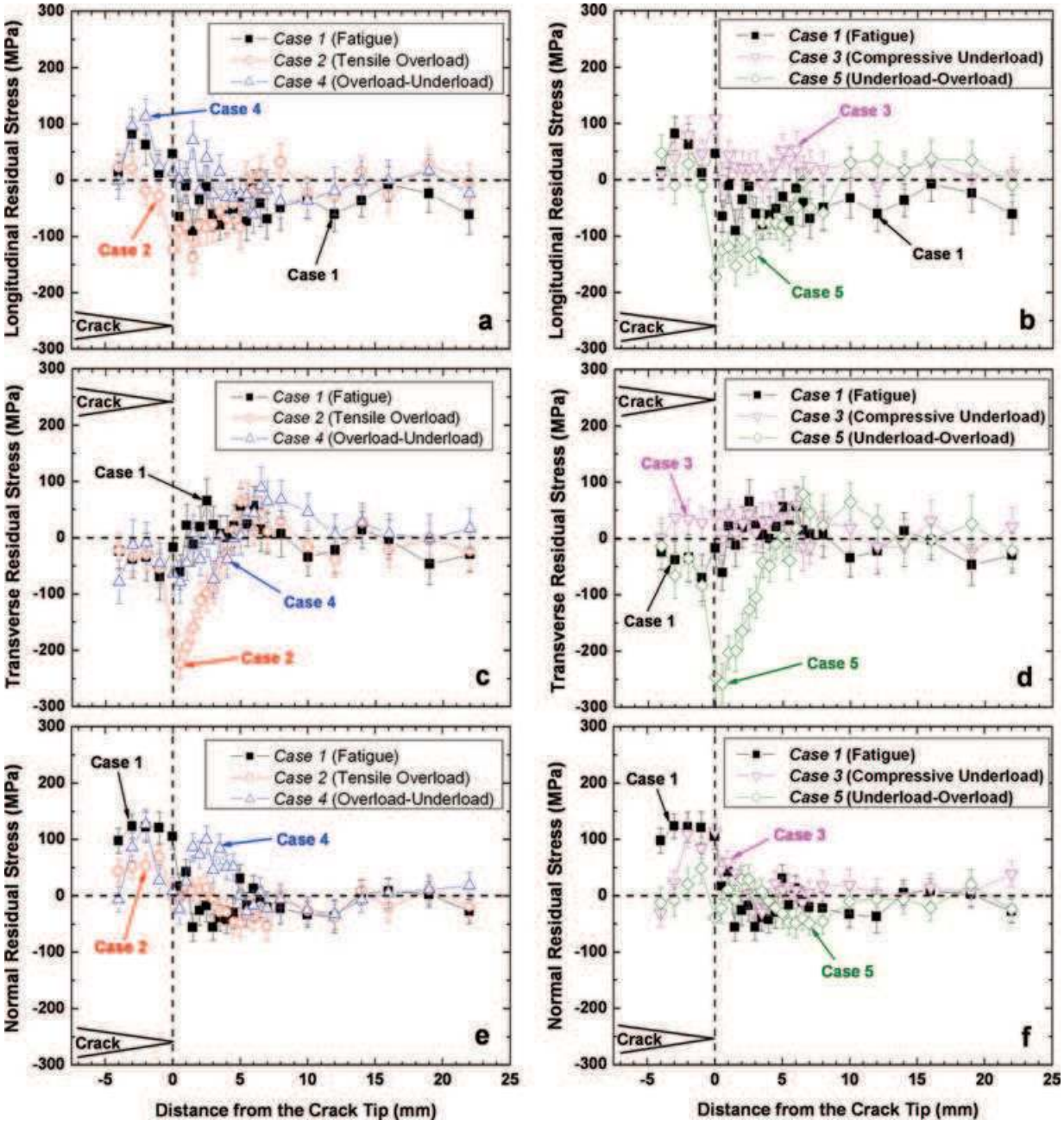

Fig. 4 Longitudinal residual-stress (σ_x) distributions as a function of the distance from the crack tip for the tests with (a) *Case 1*, *Case 2* and *Case 4*, (b) *Case 1*, *Case 3* and *Case 5*; transverse residual-stress (σ_y) distributions as a function of the distance from the crack tip for the tests with (c) *Case 1*, *Case 2* and *Case 4*, (d) *Case 1*, *Case 3* and *Case 5*; normal residual-stress (σ_z) distributions as a function of the distance from the crack tip for the tests with (e) *Case 1*, *Case 2* and *Case 4*, (f) *Case 1*, *Case 3* and *Case 5*. Note that neutron-diffraction residual stress measurements were performed immediately after various variable-amplitude fatigue loadings were applied and then unloaded, as shown in the marked circle in Fig. 2.

compressive underloading influences up to about 5 mm ahead of the crack tip.

After *Case 3* (a single compressive underload) was introduced, the longitudinal, transverse and normal residual-stress profiles were presented in Fig. 4b, d and f, respectively. It was found that a single compressive underload resulted in the small tensile residual stresses around the crack tip for the longitudinal direction (Fig. 4b). It should be noted that the slight tensile residual stresses of about 35 MPa were measured behind the crack tip for the transverse direction (Fig. 4d). A single compressive underload also led to the significant decrease of normal residual

stresses at the closer locations (e.g. −4 mm) from the initial notch.

A tensile overload was imposed immediately after the compressive underload (*Case 5*). For the longitudinal direction, the large compressive residual stresses were observed at −1 to 8 mm from the crack tip. The maximum compressive residual stress of −170 MPa was measured at the crack tip. Figure 4d revealed the large compressive transverse residual stresses around the crack tip immediately after applying underload–overload sequence. The largest compressive stress of about −260 MPa was examined at 0.5 mm in front of the crack tip. For the normal direction, the tensile residual stresses behind the crack tip was decreased and a sharp drop of residual stress at the crack tip was also observed right after the tensile overloading, which was consistent with that of *Case 2* (Fig. 4e). Overall, the residual-stress distributions of *Case 5* were very similar to those of *Case 2*, likewise, resulting in a large crack-growth retardation period, as shown in Fig. 3.

Figure 5 shows the scanning electron microscope micrographs for five different loading cases. Figure 5a and b (*Case 1*, constant-amplitude fatigue) showed crack closure in a fatigue-wake region, whereas the crack-tip blunting (Fig. 5d) was observed immediately after applying *Case 2* (a single tensile overload). When a compressive underload was introduced right after the tensile overload (*Case 4*), the distance between the fracture surface near the notch seems to increase (Fig. 5e), and the distance between the fracture surface behind of the crack tip seems to decrease (Fig. 5f), as compared to those of *Case 2* (Fig. 5c and d). However, the crack still remained open in a fatigue-wake region. On the other hand, after *Case 3* (a single compressive underload) was imposed, the open crack was observed near the notch (Fig. 5g), but the crack was completely closed behind the crack tip (Fig. 5h). When a tensile overload was applied right after the compressive underload (*Case 5*), the crack near the notch was significantly open (Fig. 5i), and the crack tip became blunt (Fig. 5j), as similarly observed in Fig. 5c and d. Moreover, the crack branching or secondary cracks occurred near the blunt crack.

The experimentally measured transient crack-growth behaviours shown in Fig. 3 might be attributed to the crack-opening load variations influenced by the combined effects of the changes in the residual-stress state and crack-tip geometry. For instance, the crack-growth retardation phenomena after the overload (*Case 2*) might be due to the changes in the crack-opening level affected by the combined contributions of crack-tip blunting and enlarged compressive residual-stress fields. Immediately after the tensile overload was applied, the large compressive residual stresses were measured near the crack tip, and the geometry of crack tip was changed from the sharp crack to blunt crack. These overload-induced enlarged compressive residual-stress fields would contribute to increasing the crack-opening level within the retardation period, although they are somewhat relaxed with the advance of the crack through the overload-plastic zone.[24] The blunt crack (with secondary cracks or branching) would also influence the increment of crack-opening level. It tends to concentrate the stresses at the blunting region rather than the actual crack-tip position, and, thus, a higher applied load would be required to make a closed crack fully open.

Note that the effects of crack-tip blunting and compressive residual stress on the crack-opening level are dependent upon the crack length propagated from the blunted region (i.e. an overload point). Moreover, the blunting effect is also influenced by the magnitude of compressive residual stress applied in the crack wake. As a result, the combined contributions of crack-tip blunting and compressive residual stress should be considered to determine the crack-opening level at each crack-propagation stage after the overload. In this aspect, the maximum retardation (the minimum crack-growth rate within the retardation period shown in Fig. 3a) can be obtained at the point where the combined contributions of crack-tip blunting and compressive residual stress are maximized. At this maximum retardation stage, it is expected that these combined effects would result in the highest crack-opening level, leading to the complete transfer of stress concentration from the blunted region to actual crack-tip position.

The application of *Case 4* (overload–underload) showed the reduced retardation period, as exhibited in Fig. 3a. It can be thought that it is mainly due to reduced transverse residual stress field by the compressive underloading. These relatively small compressive residual stresses also lessen the blunting effect. It is believed that the reduced combined effects of crack-tip blunting and compressive residual stresses result in smaller crack-opening level, and, thus, higher crack-tip driving force, as compared to those of *Case 2*. Therefore, the small retardation period would be observed for crack-growth test subjected to *Case 4*.

After *Case 3* (a single compressive underload) was applied, the crack was still closed behind the crack tip (Fig. 5h), and the slight tensile residual stresses were observed in the crack wake (Fig. 4d). It is expected that these tensile residual stresses in a fatigue wake would lead to smaller crack-opening level, and, thus, higher crack-tip driving force, which accounts for the initial acceleration immediately after a single compressive underload. A tensile overload was introduced immediately after the compressive underload (*Case 5*). It is noted that *Case 5* reveals the larger crack-growth retardation period than *Case 2*. Thus, it is obvious that *Case 3* (a single compressive underload) had the higher crack-tip driving force than that of *Case 1*. This observation might be related

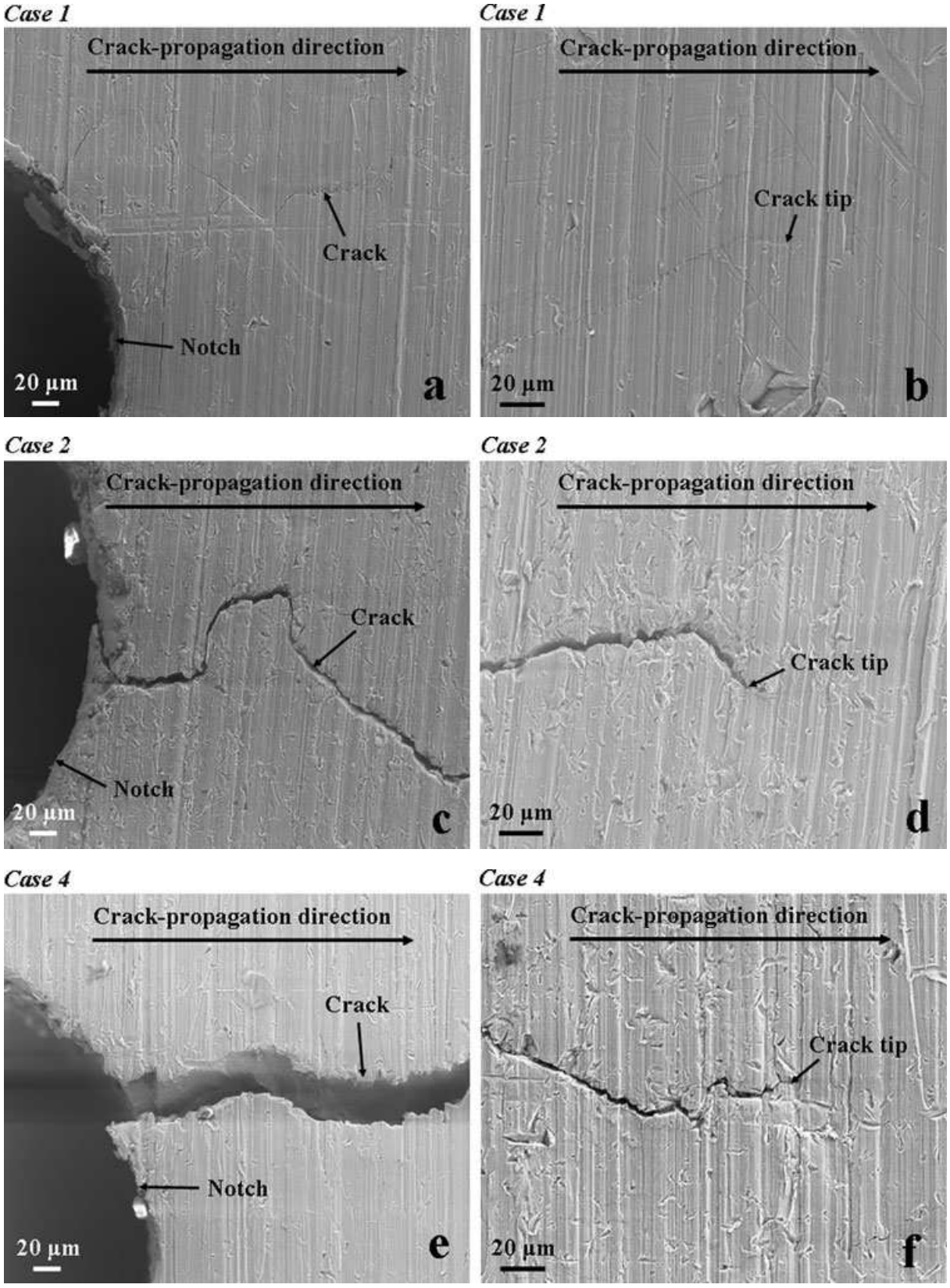

Fig. 5 SEM micrograph showing the shape of respective crack tips immediately after applying five different loading conditions. *Case 1* (a, b); *Case 2* (c, d); *Case 4* (e, f); Case 3 (g, h) and *Case 5* (i, j).

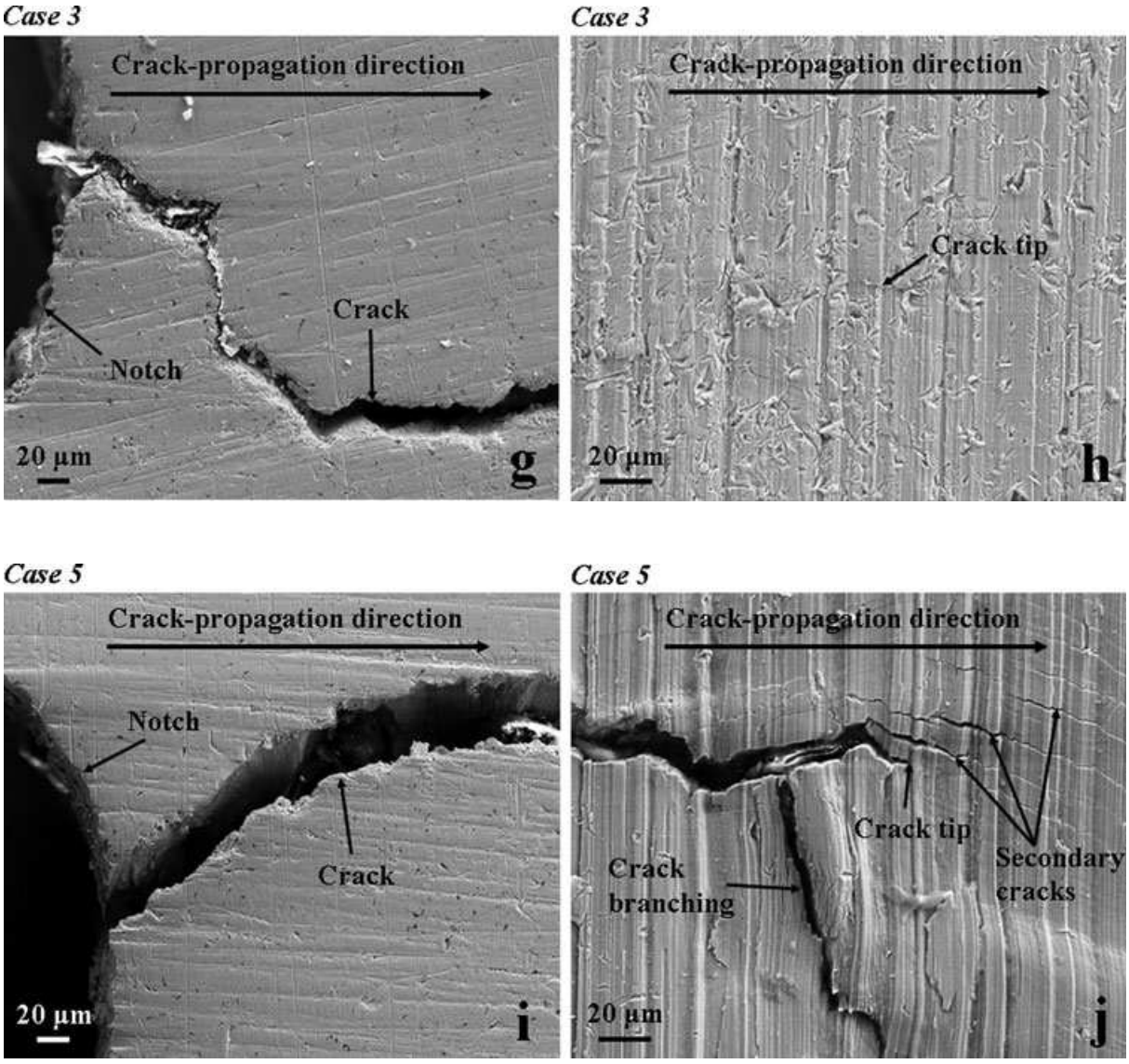

Fig. 5 Continued.

to the larger plastic deformation ahead of the crack tip by the tensile overload in *Case 5* than *Case 2*. Note that *Case 5* revealed the larger compressive residual stress (about −260 MPa) and zone (within ±5 mm from the crack tip) than those of *Case 2*. Furthermore, the crack branching or secondary cracks near the blunt crack (Fig. 5j) would promote the stress concentration at the blunting region, requiring a higher crack-opening level. Therefore, the combined contributions of crack-tip blunting (with crack branching or secondary cracks) and enlarged compressive residual stress in *Case 5* should decrease the crack-tip driving force for crack propagation, resulting in the slightly lower crack-growth rate and larger retardation period than those of *Case 2*.

SUMMARY

To investigate the distinct crack-growth characteristics subjected to tensile overload, compressive underload, and their mixed loads during fatigue crack propagation, the spatially resolved neutron residual-stress measurements were performed on five compact-tension specimens, immediately after applying various variable-amplitude loadings (i.e. fatigued, tensile overloaded, compressive underloaded, tensile overloaded–compressive underloaded, and compressive underloaded–tensile overloaded) during fatigue crack propagation. The shape of respective crack tips on the five specimens was examined using scanning electron microscope. It was found that the transverse residual-stress distributions near the crack tip revealed

the most distinct profiles, which can be closely associated with the experimentally measured different crack-growth behaviours under the five different loading cases. The significant changes in the crack-tip geometry (e.g. crack-tip blunting, crack branching or secondary cracks) was observed for *Cases 2*, *4* and *5*. It is thought that the combined effects of the changes in the residual-stress state and crack-tip geometry seem to be a key factor to account for the observed transient crack-growth phenomena.

Acknowledgements

This research is supported by the National Science Foundation (NSF), International Materials Institutes (IMI) Program under contract DMR-0231320, with Dr. U. Venkateswaran, Dr. D. Finotello, and Dr. C. Huber as the program directors. The authors appreciate National Research Council, Canada for the neutron beam time. The test materials were supplied by Haynes International, Inc. from Dr. D.L. Klarstrom. The authors would like to thank Mr. D. Fielden and Dr. M. Gharghouri for their help during experiments.

REFERENCES

1 Wardclose, C. M., Blom, A. F. and Ritchie, R. O. (1989) Mechanisms associated with transient fatigue crack-growth under variable-amplitude loading – an experimental and numerical study. *Eng. Fract. Mech.* **32,** 613–638.
2 Withers, P. J. (2007) Residual stress and its role in failure. *Rep. Prog. Phys.* **70,** 2211–2264.
3 Almer, J. D., Cohen, J. B. and Winholtz, R. A. (1998) The effects of residual macrostresses and microstresses on fatigue crack propagation. *Metall. Mater. Trans. A* **29,** 2127–2136.
4 Carlson, R. L., Kardomateas, G. A. and Bates, P. R. (1991) The effects of overloads in fatigue crack-growth. *Int. J. Fatigue* **13,** 453–460.
5 Damri, D. and Knott, J. F. (1993) Fracture modes encountered following the application of a major tensile overload cycle. *Int. J. Fatigue* **15,** 53–60.
6 Shin, C. S. and Hsu, S. H. (1993) On the mechanisms and behavior of overload retardation in Aisi-304 stainless-steel. *Int. J. Fatigue* **15,** 181–192.
7 Wheatley, G., Hu, X. Z. and Estrin, Y. (1999) Effects of a single tensile overload on fatigue crack growth in a 316L steel. *Fatigue Fract. Engng. Mater. Struct.* **22,** 1041–1051.
8 Makabe, C., Purnowidodo, A. and McEvily, A. J. (2004) Effects of surface deformation and crack closure on fatigue crack propagation after overloading and underloading. *Int. J. Fatigue* **26,** 1341–1348.
9 Su, X., Gu, M. and Yan, M. (1986) A simplified residual-stress model for predicting fatigue crack-growth behavior at coldworked fastener holes. *Fatigue Fract. Engng Mater. Struct.* **9,** 57–64.
10 Willenborg, J. D., Engle, R. M. and Wood, H. A. (1971) A crack growth retardation model using an effective stress concept, Report AFFDL-TM-71-1-FBR, Dayton (OH): Air Force Flight Dynamics Laboratory, Wright–Patterson Air Force Base.
11 Lam, Y. C. and Lian, K. S. (1989) The effect of residual-stress and its redistribution on fatigue crack-growth. *Theor. Appl. Fract. Mech.* **12,** 59–66.
12 Allen, A. J., Bourke, M. A. M., Dawes, S., Hutchings, M. T. and Withers, P. J. (1992) The analysis of internal strains measured by neutron-diffraction in Al-Sic metal matrix composites. *Acta Metall. Mater.* **40,** 2361–2373.
13 Pang, J. W. L., Holden, T. M. and Mason, T. E. (1998) In situ generation of intergranular strains in an A17050 alloy. *Acta Mater.* **46,** 1503–1518.
14 Croft, M., Zhong, Z., Jisrawi, N., Zakharchenko, I., Holtz, R. L., Skaritka, J., Fast, T., Sadananda, K., Lakshmipathy, M. and Tsakalakos, T. (2005) Strain profiling of fatigue crack overload effects using energy dispersive X-ray diffraction. *Int. J. Fatigue* **27,** 1408–1419.
15 Steuwer, A., Edwards, L., Pratihar, S., Ganguly, S., Peel, M., Fitzpatrick, M. E., Marrow, T. J., Withers, P. J., Sinclair, I., Singh, K. D., Gao, N., Buslaps, T. and Buffiere, J. Y. (2006) In situ analysis of cracks in structural materials using synchrotron X-ray tomography and diffraction. *Nucl. Instr. Meth. Phys. Res. B* **246,** 217–25.
16 Croft, M. C., Jisrawi, N. M., Zhong, Z., Holtz, R. L., Sadananda, K., Skaritka, J. R. and Tsakalakos, T. (2007) Fatigue history and in-situ loading studies of the overload effect using high resolution X-ray strain profiling. *Int. J. Fatigue* **29,** 1726–1736.
17 Lee, S. Y., Barabash, R. I., Chung, J. S., Liaw, P. K., Choo, H., Sun, Y., Fan, C., Li, L., Brown, D. W. and Ice, G. E. (2008) Neutron and X-ray microbeam diffraction studies around a fatigue-crack tip after overload. *Metall. Mater. Trans. A* **39,** 3164–3169.
18 Barabash, R., Gao, Y. F., Sun, Y. N., Lee, S. Y., Choo, H., Liaw, P. K., Brown, D. W. and Ice, G. E. (2008) Neutron and X-ray diffraction studies and cohesive interface model of the fatigue crack deformation behavior. *Philos. Mag. Lett.* **88,** 553–565.
19 Liljedahl, C. D. M., Zanellato, O., Fitzpatrick, M. E., Lin, J. and Edwards, L. (2009) The effect of weld residual stresses and their re-distribution with crack growth during fatigue under constant amplitude loading. *Int. J. Fatigue* **32,** 735–743.
20 Lee, S. Y., Choo, H., Liaw, P. K., Oliver, E. C. and Paradowska, A. M. (2009) In situ neutron diffraction study of internal strain evolution around a crack tip under variable-amplitude fatigue-loading conditions. *Scr. Mater.* **60,** 866–869.
21 Haynes Online Literature, HASTELLOY C-2000 Alloy Brochure. Available from http://www.haynesintl.com/pdf/h2118.pdf
22 ASTM Standard E647–99: Standard Test Method for Measurement of Fatigue Crack-Growth Rates, 2000 Annual Book of ASTM Standards, Vol. 03.01, pp. 591–630.
23 Rice, J. R. (1967) Mechanics of crack tip deformation and extension by fatigue. *ASTM STP* **415,** 247–309.
24 Lee, S. Y., Sun, Y., An, K., Choo, H., Hubbard, C. R. and Liaw, P. K. (2010) Evolution of residual-strain distribution through an overload-induced retardation period during fatigue-crack growth. *J. Appl. Phys.* **107,** 023517.